NANO EXPRESS

Nanomechanical Characterization of Indium Nano/Microwires

Prashant Kumar · M. S. R. N Kiran

Abstract Nanomechanical properties of indium nanowires like structures fabricated on quartz substrate by trench template technique, measured using nanoindentation. The hardness and elastic modulus of wires were measured and compared with the values of indium thin film. Displacement burst observed while indenting the nanowire. 'Wire-only hardness' obtained using Korsunsky model from composite hardness. Nanowires have exhibited almost same modulus as indium thin film but considerable changes were observed in hardness value.

Keywords Trench template method · Nanowires · Nanomechanical property

Low-dimension structures such as nanowires/dots/rods have attracted considerable interest to the scientific community in the past decade both for their size-dependent physical and chemical properties [1] and their potential in the research and development of new optoelectronic and microelectronic devices. Micro/nanodevices need conductors to provide power as well as electrical/magnetic signals to make them functional. Gold and silver are among the most useful metals for many of the micro/nanodevice applications [2]. In contrast, indium is widely used metal in devices such as contacts, thermal interface applications, solder and cold-welding applications, because of its excellent malleability, high thermal and electrical conductivities, compressibility, and ease of application. Indium nanowires have peculiar temperature-dependent electrical properties; which make them attractive for various applications [3]. In particular, under the superconducting temperature, the electrical resistance of indium nanowires rapidly decreases, which is expected to play an important role in making magnetic field generators or superconducting quantum-interference devices [4]. Synthesis and the temperature-induced metal–insulator transitions of indium nanowire arrays on silicon substrate have been reported earlier [5–9]. In addition, indium nanoparticles have also attracted intensive interest because they can be used as lubricants, single-electron transistors and tags for the detection of DNA hybridization [10–13].

Although indium nanowires have been successfully synthesized by various techniques such as porous alumina template by hydraulic pressure injection technique [14, 15] for luminescence applications, potentiostatic stationary electrodeposition from an $InCl_3$-based solution [16], single crystal indium nanowires using ultrafast rate by focused ion beam (FIB) [3], their mechanical properties have not been discussed much. Mechanical and structural aspects are of great importance in developing nanoscale building blocks into functional nano/microdevices in determining the long-term stability and reliability. Most mechanical properties are known to exhibit a dependence on specimen size [17–19]. Currently, many potential applications for these micro/nanoscale structures are not really practical because their mechanical properties have not been established [17–21]. A promising approach for measuring the mechanical properties of such nanostructures is direct nanoindentation [22–27].

Current author has employed trench template–assisted vapour condensation technique to fabricate long nanowires inside the trench [28–30]. Such a technique is extremely

P. Kumar (✉)
Jawaharlal Nehru Centre for Advanced Scientific Research,
Bangalore 560 064, India
e-mail: prashantkumar@jncasr.ac.in

M. S. R. N Kiran
Department of Materials Engineering, Indian Institute of
Science, Bangalore 560 012, India

useful in the sense; it yields nanowire growth at a desired position and eliminates the need of any post-fabrication manipulation. We report, for the first time to our knowledge, the hardness and elastic modulus of indium nanowires (different diameters) fabricated by trench template method using nanoindentation technique.

Indium nano/microwires were fabricated inside the V-trench (2–20 μm diameter, 100–200 nm depth) templates scribed by electronically controlled diamond scriber with the provision of load selection on thoroughly cleaned quartz substrate by vapour condensation (thermal evaporation) at high vacuum (1×10^{-6} mbar). The process of formation of nanowire inside the trench template has been described in detail elsewhere [28–30].

The morphology of the features grown inside the trenches was determined using atomic force microscope (SPA 400 of SII Inc., Japan) operating in the non-contact dynamic force microscopy (DFM) mode. The hardness and elastic modulus of indium films and nanowires were measured using a nanoindenter (Triboindenter of Hysitron, USA, Minneapolis) with in situ AFM imaging capability. The machine monitors continuously and records the load and displacement the diamond indenter during indentation with a force resolution of about 1 nN and a displacement resolution of about 0.2 nm.

The indenter tip was used to image and locate indium nanowires and then in situ indent on the wire with the same tip. Extreme care should be taken at this point to avoid tip break/damage. Post-indent impression was captured using the same tip. Post-test imaging provides the ability to verify that the test was performed in the desired location, which improves the reliability of the data and aids in the explanation of unexpected test results. To avoid thermal drift effects, sufficient time (3–4 h) has been provided to system after switching on the machine to achieve thermal equilibrium conditions. The machine allows shallow penetration depths ($\sim$5 nm) because it is inherently a load control instrument with its extremely low noise floor.

Values of hardness and elastic modulus were obtained using the Oliver and Pharr [31, 32] method of fitting to the initial part of the unloading curve. The load was increased and decreased in a linear fashion in this experiment. A 3-sided pyramidal diamond Berkovich tip with a tip radius of 50 nm was used for indentation on the films. Indents were made at different loads varying from 100 to 1200 μN. Two different loading functions have been used in this study. First one, a triangular loading function (10 s load-10 s hold- 10 s unload)—used to observe whether any pop-in or pop-out effects occur. At the peak loads, the hold time was kept at 10 s to determine creep effects in the films. Second one, a partial unloading function (50% unloading at the peak load) was used to obtain depth-dependent hardness of the film/wire between the loading ranges from 0 to 500 μN.

Trench-templated deposition was carried out without any external heating and at very slow rate of deposition (1–4 A°/s). Summarizing, the parameters which decide [35–37] the diameter of the nanowire so formed are trench width, trench depth, evaporation source–substrate distance, tungsten filament length apart form the rate of deposition, substrate temperature, material of deposition, substrate material and its surface roughness. Lower rate of deposition is desired where material transfer to the substrate will not cause any agglomeration. Lower substrate temperature is desired for avoiding surface diffusion of adatoms while first few layers are formed. Total surface energy available when condensate atoms land on the substrate surface should be favourably minimum for the formation of nanowires. For all other parameters fixed, trench width/ trench depth ratio (W/H) is the determining factor for the extent of shadowing. There exists a window of W/H which favours organized assembled growth in the form of organized nanodots or nanowires. Shadowed area has restricted vapour supply which gives rise to dewetting. Dewetting along with the directionality imposed by the geometry of trench results in the formation of nanowire or organized nanodots inside the trench template.

It has been reported earlier that indium nanowire sample shows nanocrystalline peak corresponding to [112] and [202] crystallographic planes and do belong to cubic lattice system [29]. The absence of any known peaks corresponding to indium oxide in x-ray diffractogram reveals that the film/wire was not oxidized immediately.

For the 200 s indium coating (with film thickness of 100 nm as calculated from time and rate of deposition), nanoparticulated growth features with average grain size in the range of 130–250 nm were observed onto 30-nm continuous thin film layer as shown in Fig. 1a. Inside the trench template, nanoparticles organize by self-assembly to an organized manner in the form of nanowires, shown in Fig. 1b. Nanowires form on the sidewalls of the trench template as shown in the inset of Fig. 1b. Straightness is a concern for the indium metal [29] when compared to that for the nickel and gold [28]. This kind of behaviour for indium especially may be due to its adhesion coefficient and its low melting point. The difference in the vapour temperature (as it depends on the heat transferred by the tungsten filament to the indium material while heating and vaporizing) and the solidification temperature will decide the resulting surface feature apart from the other factors (substrate material, surface roughness, etc.). From Fig. 1b, it is clear that there are three different diameters of (i.e. 500, 1200 and 2000 nm) wires grown in the trench. The diameters of the wires are larger in the present study because trenches were made on quartz substrates by usual diamond scriber which had higher diamond tip diameter. Experiments are underway to controllably fabricate

Fig. 1 Atomic Force Microscope (operated in intermittent non-contact mode) image of **a** continuous indium film on quartz substrate **b** indium nanowires grown inside the trench template (*shown in red coloured arrows*) [*up right inset* in **b** shows the schematic diagram of the technique and *down right inset* shows the growth of nanowires in a trench], **c** residual indent impression of Indium nanowires (contrast of the image was improved using Microsoft Office Picture Manager software in order to show a clear indent impression on wire kind of structure), **d** the line profile of the indent, **e** Coloured 3-D image of indented impression
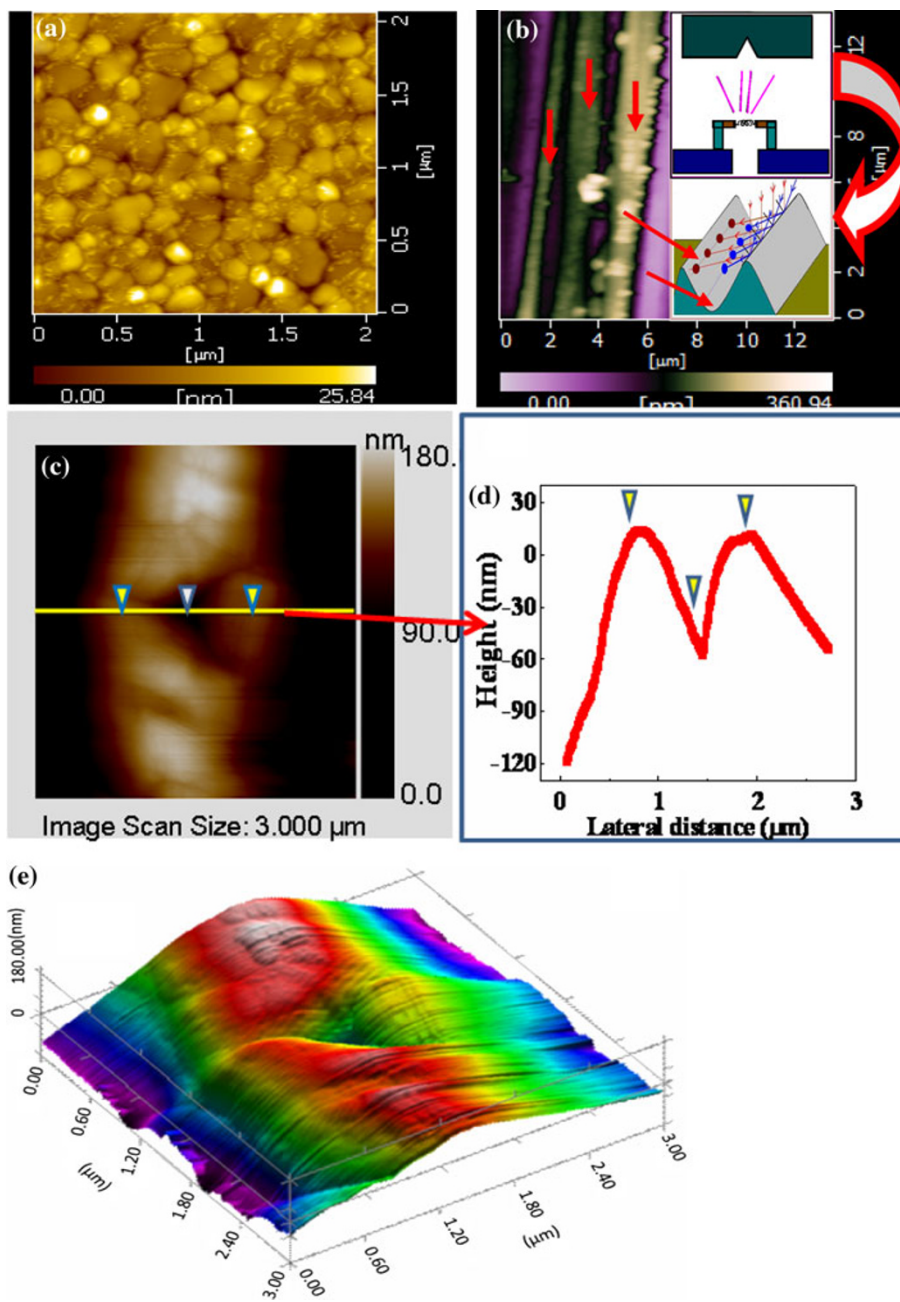
nanowires of diminished diameter to exploit its size-dependent behaviour.

Figure 1c shows the AFM image of the indent on the flat wire of diameter 2000 nm and the total height of 100–180 nm. Figure 1d shows the line profile of the indented impression. Figure 1e is a coloured 3D image for the residual indent impression on the same nanowire shown in Fig. 1c. The peak nanoindentation depth can be as low as 50 nm (for 500 nm dia wire), which is about 10% of the wire diameter. In our case of experimentation, height of nanowire/microwire is found to be 100–180 nm which is in safe zone. In general, the depth of indentation should not cross more than 10% of the film/wire thickness to avoid substrate effects in the hardness/modulus data. The same Berkovich tip was used to perform indentation test as well as for imaging after indentation. Indenting on a wire kind of structures is a bit difficult because under high load, wire can move/roll on the substrate surface hence indenter slips. Slipping of the indentation tip onto the wire top surface has been tried to avoid by placing indenter tip just midway on the top of the nano/microwire. In the present case, the adhesion forces between the wires and quartz substrate are strong enough to avoid wire from moving/rolling on the substrate. Interestingly, no cracking or chipping was

observed and only some pile-up observed on either side of the residual indent in the nanowires case. But under the same load, indium film did not show any pile-up effects. However, the pile-up height is very less in the wire case. Pile-up correction has been done to the hardness and modulus data obtained from Oliver–Pharr method. Depending upon strain hardening of the tested material, the surface deformation mode of an indent can be pile-up or sink-in. In low strain-hardening materials, pile-up tends to occur due to incompressible plastic deformation. The opposite is true for high strain-hardening materials [31]. From the above analysis, it is clear that nanowire exhibits more plastic-like behaviour. Additionally, the indenter has penetrated up to the substrate surface at higher loads, but there was no sign of radial crack formation of the film/wire. It means that indium wires are in good adhesion towards the substrate. To confirm the values of indentation hardness calculated from Oliver–Pharr method, we have calculated hardness using indentation projected area obtained from residual indent in the AFM image. Indentation-projected area calibration eliminates the wire curvature effects on the mechanical properties. Both the methods have resulted different values of hardness.

Load–displacement (L-D) curves for nanowire sample and untemplated continuous thin film are as shown in Fig. 2. Figure 2a shows the L-D curve of indium thin film. While indenting smaller structures at nanoscale (particularly nanowires kinds of structures), it is very difficult to avoid hitting the smaller particles on the wire surface. Figure 2 depicts how load–displacement curve will be affected by hitting the particles available on the surface. In Fig. 2a, indenter did not encounter any particles, and the

response is that of the indium films. Figure 2b, however, the indenter tip pushes first through a particle approximately 20–25 nm thick before encountering the hard surface. The very low slope of these initial loading curves indicates that the particles are much softer than the indium nanowires beneath [32]. When we perform displacement off-set to 25 nm, then the loading part exactly fits to Hertzian contact equation.

This phenomenon of 'pop-in' (displacement burst or strain burst) was attributed to very poor defect density prior to nanoindentation test so that the onset of plasticity requires load sufficient for dislocation nucleation and propagation. In indium nanowires, the pop-in occurred at about 35 μN load and at 40 nm depth, as shown in Fig. 2b. Shortly, after the first displacement burst, the load–displacement curve becomes serrated as shown in Fig. 2b, indicating series of small displacement bursts followed by the main one. At larger loads, these serrations disappears [33]. The small amount of pile-up around the indenter could be because of these many number of small displacement bursts. No crack formation at the indenter edges was observed in the present study. In the previous studies [34], the displacement burst in indium thin films observed at 120 μN. But in the present case, pop-in occurred at very low load which might be because of the existence of poor defect density of mobile dislocations and also they require higher amount of stress to start dislocation nucleation and propagation in the nanowires. This pop-in behaviour in metals and ceramics is often correlated to either the nucleation of dislocations in a perfect crystal or the rapid multiplication of dislocations from a limited source population.

The shear modulus of indium nanowire is 4.5 GPa calculated from effective elastic modulus, E_{eff}, of indium films ($\sim$50 GPa), obtained from Oliver–Pharr method and poison's ratio υ_f ($\sim$0.3). The theoretical shear strength τ_T for the indium nanowires is 1.0 GPa. Using the above equations, the maximum shear stress calculated at which first pop-in occurred was 930 MPa for indium wire sample. Almost theoretical shear strength and maximum shear stress at which pop-in occurred are almost matching, and the very small difference between τ_m and τ_T is due to the experimental scatter, residual stresses in wire, defects and surface roughness. Occurrence of several discontinues in L-D curve indicates that the dislocation sources generated during the displacement burst are not very stable and unable to operate continuously at relatively low stress levels, throughout the entire-elastic–plastic loading.

To understand the time-dependent plastic deformation (creep) of the indium film and wire, a hold time of 10 s kept at a peak load of 100 μN. Indium wire crept significantly during hold load than indium film. It can be seen from Fig. 2a that the displacement was also creeping
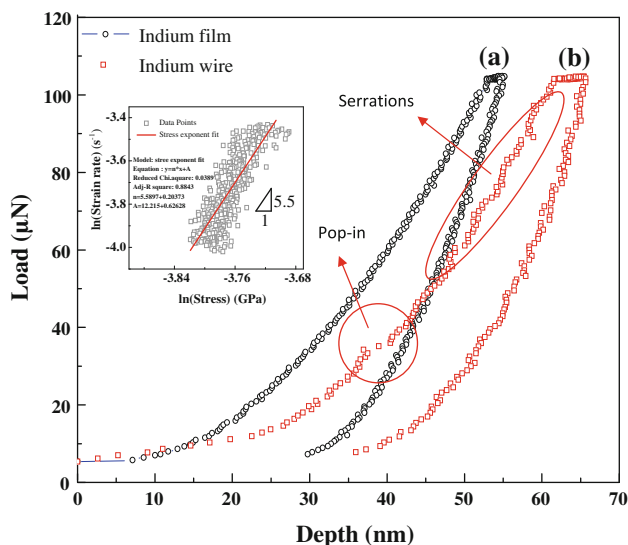
Fig. 2 The behaviour of load–displacement curves for **a** indium film, **b** indium wire. [*Inset*: Plot between ln(strain rate) and ln(stress), to find out the stress exponent of the indium wire]

during the hold time, even though no strain burst had taken place. The inset of the Fig. 2 shows the ln(strain rate) vs ln(stress) plot for the nanowires sample. The stress exponent obtained for the nanowires sample was 5.5 calculated from the slope of the curve. According to Feng et al. [35], the creep behaviour of indium is distinctively different from other metals. For example in aluminium, pop-in is a pre-requisite for an indentation creep. However, for indium, creep can happen before or after pop-in. The stress exponent before and after the pop-in was also remarkably different—it changes from ∼1.5 before pop-in ∼6 after pop-in. Lucas and Oliver [36] have reported the value of stress exponent was 5–7 for indium films after pop-in. The value of ∼1.5 before displacement burst is rather low compared with the usual range expected for dislocation creep, which is 3–8. They have concluded that before strain burst, it was diffusional creep, and after displacement burst, it was dislocation creep. Diffusional creep can happen at the test temperature because room temperature is 0.7 T_m for indium. Our results on stress exponent are also matching with the reported values. From the above analysis, it is understood that the onset of dislocation creep phenomena occurs in indium nano/microwire kind of structures at much lower loads (30–40 μN) compared to bulk/thin indium films (80–120 μN). This could be attributed to the better crystalline quality and low dislocation density of the indium wire kind of structures.

Nanomechanical properties such as indentation hardness and modulus of the indium wires and thin film calculated from the load–displacement curves using Oliver–Pharr method after pile-up correction are shown in Fig. 3. The hardness and elastic modulus of the film as well as wire as a function of normalized depth is presented in Fig. 3a. This data was obtained using partial unloading function. It is clear that the effect of substrates has come into picture after a critical film/wire thickness. To find out 'film/wire-only hardness' from the composite hardness (film + substrate), we have used Korsunsky's equation to fit the experimental data. For soft films on hard substrates, the reduced modulus can increase with indentation depth. Both the reduced modulus and hardness measurements are influenced by the substrate. The hardness value for the indium continuous film after the Korsunsky fit was 2.55 GPa, whereas it was 1.99 GPa for the nanowires of diameter ∼2000 nm. The hardness of quartz substrate was taken as 10 in the above
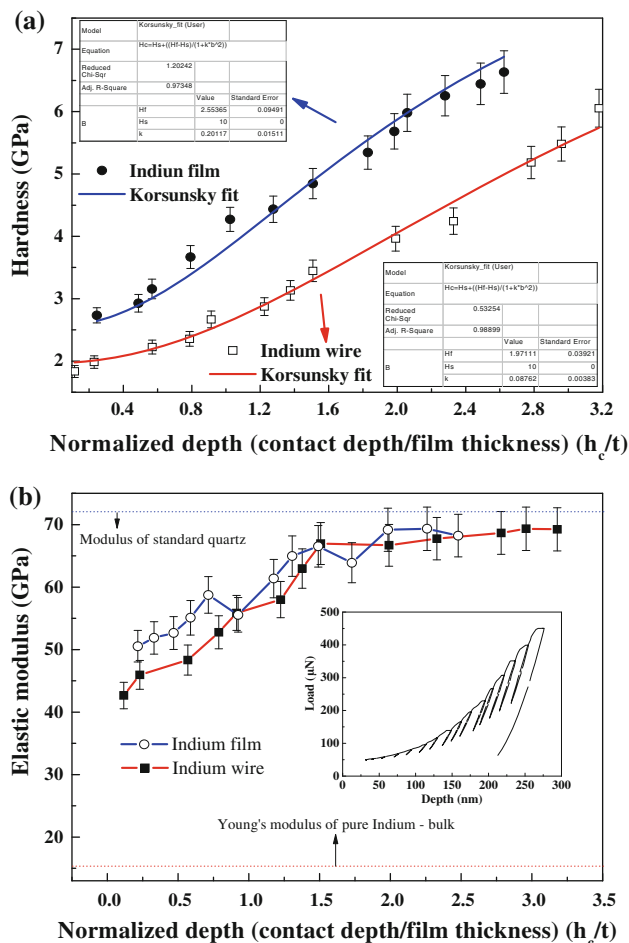
Fig. 3 The trends for indium film and nanowire with the normalized depth for **a** hardness and **b** elastic modulus [*Inset*: Partial unloading function used to obtain depth-dependent mechanical properties of nanowires at a single spot]

equation. The hardness of the 500 nm diameter of nanowire was found to be 1.4 GPa. After the indentation projected area calibration, the hardness values of the indium thin film and wires were measured to be about 2.15 ± 0.5 and 1.3 ± 0.4 GPa, respectively. Not much difference in the hardness of the different diameter wires was observed. The values of hardness and modulus of wires have been tabulated in Table 1. The differences between these two methods could be due to the pile-up phenomenon. Oliver and Pharr's proposed method is best applied when no pile-up but some sink-in occurs when the sample is indented. In

Table 1 Summarizes the variation of mechanical properties of nanowires of different diameters and comparison with the indium thin film

Sample	Load (μN)	Max. depth (nm)	Hardness (GPa) (O–P method)	Reduced modulus (GPa)
Wire diameter = 500 nm	50	40	1.62 ± 0.214	37 ± 4
Wire diameter = 2000 nm	100	65	1.99 ± 0.039	40 ± 4
Untemplated continuous Indium thin film (100 nm)	100	55	2.55 ± 0.094	55 ± 5

the case of pile-up, contact depth is always more than the total depth of indentation, thus the projected area is always underestimated. This underestimated area could overestimate both hardness and reduced elastic modulus, with a more significant effect on hardness [37].

Trend with the normalized depth for elastic modulus is shown in Fig. 3b. Elastic Modulus is a measure of stiffness of a material. In the present case of indium metal, indium nanowire and untemplated continuous thin film, both show almost same kind of behaviour but the value of elastic modulus for the film was a bit higher than the wire. Film exhibited the value of modulus around 50 GPa and it was 40 GPa for the wire of diameter 2000 nm. Even the modulus of the 500-nm-diameter wire exhibited still lower modulus than 2000-nm-diameter wire but the difference was not much. The elastic modulus of the indium wire decreases as its diameter decreases, because of lateral deformation of the wire. Increasing the penetration depth will increase the lateral deformation and in turn significantly decreases the elastic modulus of the wire. Several reports have demonstrated the results of size-dependent elastic modulus of nanowires. They found that the elastic modulus can increase, decrease or not change with decreasing wire diameter [38]. There are two possibilities to explain the phenomenon. One is the surface modification which could arise from the change of the surface tension of the nanowires and decreasing diameter due to the large surface-to-volume ratio; another is the change of crystallographic directions in the nanowires that also alter their elastic modulus. Chang et al. [39–45] have suggested that the smaller diameter nanowires could not provide sufficient elastic force to resist the pressure from the indenter in the unloading process, yielding the lower contact stiffness, resulting in the lower modulus. Besides, the nanowires subjected to nanoindentation could have the lateral deformation behaviour, which also affects the estimate of the elastic modulus [46]. Recent report [47] has also revealed that the elastic modulus of silicon nanowires is unaffected by their sizes, and their young's moduli of wires are close to that of bulk modulus. In our case, it should be noted that the dimension of our indium nanowires are much larger than the critical dimension at which the surface effect does play an important role on elastic properties of nanowires.

In conclusion, nanomechanical properties of trench template–fabricated indium nanowires have been measured by directly indenting the wires. It is observed that elastic modulus and hardness were found be less for indium wires than indium continuous films. It is found from the creep studies that in the case of nanowires, onset of dislocation creep phenomena occurs at very low loads. Hardness and modulus of indium micro/nanowires decrease with the decrease in wire diameter. To our knowledge, this is the first report on the mechanical properties of indium nanowires fabricated by trench template method and using nanoindentation technique.

Methodology

The hardness of a material is defined as its resistance to local plastic deformation [48, 49]. Thus, indentation hardness, H, can be determined from the maximum indentation load, P_{max}, divided by the contact area, A:

$$H = P_{max}/(A) \tag{1}$$

where the contact area (A) is a function of the penetration depth, h, and can be determined by the following equation:

$$A(h) = C_0 h^2 + C_1 h + C_2 h^{1/2+} C_3 h^{1/4} + \cdots + C_8 h^{1/128} \tag{2}$$

It may be noted that only the constant C_0 is used, if it is assumed that a Berkovich indenter has a perfect tip. However, for imperfect tips, higher-order terms have to be taken into account and these are obtained from the tip-area function curve fit for a given tip. In the current case, the values are $C_0 = 24.5$, $C_1 = -2.3425 \times 10^3$, $C_2 = 2.764 \times 10^5$, $C_3 = -2.9845 \times 10^6$, $C_4 = -3.4532 \times 10^6$ and $C_5 = -2.6574 \times 10^6$. The elastic modulus, E, of the thin film can be obtained using the following equation:

$$1/E_r^* = \left[(1 - v_i^2)/E_i \right] + \left[(1 - v_s^2)/E_s \right] \tag{3}$$

where v and E are Poisson's ratio and elastic modulus, respectively; and the subscripts i and s refer to the indenter and test material, respectively. The indenter properties used in this study are $E_i = 1140$ GPa, and Poisson's ratio for the indenter is $v_i = 0.07$. E_r^* is the reduced modulus that accounts for the fact that elastic deformation occurs in both the sample and the indenter and it can be determined from the equation

$$E_r^* = \left\{ (\pi)^{1/2}/\beta S \right\}/2(A)^{1/2} \tag{4}$$

where S is the stiffness of the test material, which can be obtained from the initial unloading slope by evaluating the maximum load and the maximum depth, i.e., $S = dP/dh$. β is a shape constant that depends on the geometry of the indenter and is 1.034 for the Berkovich tip. The contact depth can be estimated from the load–displacement data using

$$h_c = h_{max} - (\varepsilon P_{max}/S) \tag{5}$$

where ε is a constant that depends on the indenter geometry ($\varepsilon = 0.75$ for Berkovich indenter) and h_{max} the displacement at the peak load.

The loading curve can be fitted with the following power-law relation,

$$P = \alpha h^m \qquad (6)$$

and unloading curve can be expressed as

$$P = \alpha \left(h - h_f\right)^m \qquad (7)$$

where P is the indenter load, h is the elastic displacement of the indenter, h_f is the final depth, α and m are fitting constants. The value of m for Berkovich tip will be usually 1.5.

The maximum shear stress, $\tau_{\max}$, can be expressed through the mean contact pressure (P_a) as following from Hertz contact theory [50],

$$\tau_{\max} = 0.465 P_a = 0.465 \left[(4 E_{\mathrm{eff}})/3\pi\right](h_c/R)^{1/2} \qquad (8)$$

where an indentation load ($P_{\max}$) and the penetration depth (h_c) at known tip radius of the indenter or effective elastic modulus of films (E_{eff}). The theoretical shear strength τ_T of indented materials may be approximated as [51, 52]

$$\tau_T = \mu_s/2\pi = E_{\mathrm{eff}} / \left\{4\pi\left(1 + v_f\right)\right\} \qquad (9)$$

where μ_s is the shear modulus.

Korsunsky's model is based on energy expenditure during an indentation, and the final equation is given by [53]

$$H_c = H_s + \left(H_f - H_s\right)/1 + k\beta^2)$$

where β is the relative indentation depth, k is a constant related to the film thickness, H_f is film hardness, H_s is the substrate hardness and H_c is the composite hardness.

References

1. J.L. Li, X.J. Liang, J.F. Jia, X. Liu, J.Z. Wang, E.G. Wang, Q.K. Xue, Appl. Phy. Lett. **79**, 2827 (2007)
2. H. Li, C. Liang, M. Liu, K. Zhong, Y. Tong, P. Liu, G.A. Hope, Nanoscale Res. Lett. **4**, 47 (2009)
3. S.S. Oh, D.H. Kim, M.W. Moon, A. Vaziri, M. Kim, E. Yoon, K.H. Oh, J.W. Hutchinson, Adv. Mater. **20**, 1093 (2008)
4. N. Giordano, Phys. Rev. Lett. **61**, 2137 (1988)
5. J.R. Ahn, J.H. Byun, J.K. Kim, H.W. Yeom, Phys. Rev. B. **75**, 033313/1 (2007)
6. K. Fleischer, S. Chandola, N. Esser, W. Richter, J.F. Mcgilp, W.G. Schmidt, S. Wang, W. Lu, J. Bernholc, Appl. Surf. Sci. **234**, 302 (2004)
7. S. Wippermann, W.G. Schmidt, A. Calzolari, M.B. Nardelli, A.A. Stekolnikov, K. Seino, F. Bechstedt, Surf. Sci. **601**, 4045 (2007)
8. A.A. Stekolnikov, K. Seino, F. Bechstedt, S. Wippermann, W.G. Schmidt, A. Nardelli, M. Buongiorno, Phy. Rev. Lett. **98**, 26105/1 (2007)
9. J.L. Li, X.J. Liang, J.F. Jia, X. Liu, J.Z. Wang, E.G. Wang, Q.K. Xue, Appl. Phys. Lett. **79**, 2826 (2001)
10. Y.B. Zhao, Z.J. Zhang, H.X. Dang, J. Phys. Chem. B **107**, 7574 (2003)
11. K. Hitzbleck, H. Wiggers, P. Roth, Appl. Phys. Lett. **87**, 093105/1 (2005)
12. H. Yu, P.C. Gibbons, K.F. Kelton, W.E. Buhro, J. Am. Chem. Soc. **123**, 9198 (2001)
13. F.Y. Wu, C.C. Yang, C.M. Wu, C.W. Wang, W.H. Li, J. Appl. Phys. **101**, 09G111/1 (2007)
14. F. Chen, A.H. Kitai, J. Lumin **128**, 1856 (2008)
15. F. Chen, A.H. Kitai, J. Nanosci. Nanotechnol. **8**, 4488 (2008)
16. G. Hautier, P. Vereecken, K. D'Haen, K. Maex, Electrodeposited single crystalline indium nanowires, 209th ECS Meeting, ECS, 2006. pp. 86; (7–11 May, Denver, CO, USA) (2006)
17. X. Li, B. Bhushan, K. Takashima, C.W. Baek, Y.K. Kim, Ultramicroscopy **97**, 481 (2003)
18. X. Li, B. Bhushan, Surf. Coat. Technol. **164**, 503 (2003)
19. M.A. Haque, M.T. Saif, Proc. Nat. Acad. Sci. **101**, 6335 (2004)
20. X. Li, B. Bhushan, Mater. Char. **48**, 11 (2002)
21. B. Bhushan, X. Li, Int. Mater. Rev. **48**, 125 (2003)
22. X. Li, P. Nardi, C.W. Baek, J.M. Kim, Y.K. Kim, J. Micromech. Microeng. **15**, 551 (2005)
23. Z.L. Wang in Mechanical Properties of Nanowires and Nanobelts in Dekker Encyclopedia of Nanoscience and Nanotechnology. doi:10.1081/E-ENN 120013387, 1773 pp. (2004)
24. X. Li, X. Wang, Q. Xiong, P.C. Eklund, Nano Lett. **5**, 1982 (2005)
25. X. Li, H. Gao, C.J. Murphy, K.K. Caswell, Nano Lett. **3**, 1495 (2003)
26. X. Li, H. Gao, C.J. Murphy, L. Gou, Nano Lett. **4**, 1903 (2004)
27. G. Feng, W.D. Nix, Y. Yoon, C.J. Lee, J. Appl. Phys. **99**, 074304 (2006)
28. P. Kumar, M.G. Krishna, A.K. Bhatnagar, A. Bhattacharya, Int. J. Nanomanufacturing **2**, 477 (2008)
29. P. Kumar, J. Nanopart. Res. doi:10.1007/s11051-009-9813-9
30. M.G. Krishna, P. Kumar, Non-lithographic techniques for nanostructuring thin films and surfaces. in *Emerging nanotechnologies in manufacturing*, ed. by W. Ahmed, M.J. Jackson (William Andrews Inc, Academic Press, New York), ISBN 97808155 15838 (2009)
31. T.H. Fang, W.J. Chang, Microelectron. Eng. **65**, 231 (2003)
32. J.O. Carneiro, V. Teixeira, A. Portinha, S.N. Dub, R. Shmegera, Rev. Adv. Mater. Sci. **7**, 83 (2004)
33. W.M. Huang, J.F. Su, M.H. Hong, B. Yang, Scr. Mat. **53**, 1055 (2005)
34. J.H. Edgar, C.H. Wei, D.T. Smith, T.J. Kistenmacher, W.A. Bryden, J. Mater. Sci. **8**, 307 (1997)
35. G. Feng, A.H.W. Ngan, Scr. Mat. **45**, 971 (2001)
36. B.N. Lucas, W.C. Oliver, Metall. Mater. Trans. A **30**, 601 (1999)
37. S.S. Samandari, K.A. Gross, Acta Biomater. **5**, 2206 (2009)
38. C.Q. Chen, Y. Shi, Y.S. Zhang, J. Zhu, Y.J. Yan, Phys. Rev. Lett. **96**, 075505 (2006)
39. S. Cuenot, C. Fretigny, S.D. Champagne, B. Nysten, Phys. Rev. B **69**, 165410 (2004)

40. E.P.S. Tan, Y. Zhu, T. Yu, L. Dai, C.H. Sow, V.B.C. Tan, C.T. Lim, Appl. Phys. Lett. **90**, 163112 (2007)
41. L.G. Zhou, H. Huang, Appl. Phys. Lett. **84**, 1940 (2004)
42. H. Liang, M. Upmanyu, Phys. Rev. Lett. **71**, 241403 (2005)
43. E.W. Wong, P.E. Sheehan, C.M. Lieber, Science **277**, 1971 (1997)
44. B. Wu, A. Heidelberg, J.J. Boland, Nat. Mater. **4**, 525 (2005)
45. K.R. Pirota, E.L. Silva, D. Zanchet, D. Navas, M. Vazquez, M.H. Velez, M. Knobel, Phys. Rev. B **76**, 233410 (2007)
46. N.K. Chang, Y.S. Lin, C.Y. Chen, S.H. Chang, Thin Solid Films **517**, 3695 (2009)
47. Y.S. Sohn, J. Park, G. Yoon, J. Song, S.W. Jee, J.H. Lee, S. Na, T. Kwon, K. Eom, Nanoscale Res. Lett. **5**, 211 (2010)
48. W.C. Oliver, G.M. Pharr, J. Mater. Res. **7**, 1564 (1992)
49. W.C. Oliver, G.M. Pharr, J. Mater. Res. **19**, 3 (2004)
50. D. Lorenz, A. Zeckzer, U. Hilpert, P. Grau, H. Johansen, H.S. Leipner, Phys. Rev. B **67**, 172101 (2003)
51. T.H. Courtney, *Mechanical Behavior of Materials*, (McGraw Hill, New York, 2000)
52. S.R. Jian, T.H. Fang, D.S. Chuu, Appl. Surf. Sci. **252**, 3033 (2006)
53. A.M. Korsunsky, M.R. McGurk, S.J. Bull, T.F. Page, Surf. Coat. Technol. **99**, 171 (1998)